

DATA ANALYSIS METHODS FOR THE DETECTION OF THE EPOCH OF REIONIZATION

CARINA CHENG¹, ET AL.

¹Astronomy Dept., U. California, Berkeley, CA

ABSTRACT

The Epoch of Reionization (EoR) is an uncharted era in our Universe’s history during which the birth of the first stars and galaxies led to the ionization of neutral hydrogen. This important epoch of our cosmic dawn harbors a wealth of information regarding the environment during this transformative time, including insight into the nature of the first luminous sources and implications about cosmological parameters. There are many experiments investigating the EoR by tracing the 21 cm line of neutral hydrogen, a signal which is very faint and difficult to isolate. With a new generation of instruments and a statistical power spectrum detection in our foreseeable future, it has become increasingly important to develop techniques that help maximize sensitivity and validate results. Additionally, it is imperative to understand the trade-offs between different methods and their effects on common power spectrum themes. In this paper, we focus on three major themes - signal loss, power spectrum error bar estimation, and bias in measurements. We describe techniques that affect these themes using both a toy model and data taken by the 64-element configuration of the Donald C. Backer Precision Array for Probing the Epoch of Reionization (PAPER).

1. INTRODUCTION

By about one billion years after the Big Bang, the very first stars and galaxies are thought to have ionized all the neutral hydrogen that dominated the baryonic matter content in the early Universe. This transition period, during which the first luminous structures formed from gravitational collapse and began to emit intense radiation that ionized the cold neutral gas into a plasma, is known as the epoch of reionization (EoR). The EoR is a relatively unexplored era in our cosmic dawn. Its history encodes important information regarding the nature of the first galaxies and the processes of structure formation. Direct measurements of the EoR would unlock powerful information about the intergalactic medium, revealing connections between the smooth matter distribution exhibited via cosmic microwave background (CMB) studies and the highly structured web of galaxies we observe today.

One promising technique to probe the EoR is to target the 21 cm wavelength emission that is emitted by neutral hydrogen via its spin-flip transition. This technique is powerful because it can be observed as a function of redshift — that is, the wavelength of the signal reaching our telescopes can be directly mapped to a distance from where the emission originated before stretching out as it traveled through expanding space. The 21 cm line therefore offers a window into the evolution of ionization, temperature, and density fluctuations on cosmic scales.

Although a detection of the EoR remains elusive, there are several radio telescope experiments that have succeeded in using the 21 cm signal from hydrogen to place constraints on the brightness of the EoR. Ex-

amples of experiments investigating the mean brightness temperature of the EoR relative to the CMB are EDGES ([Bowman & Rogers 2010](#)), the LWA ([Ellingson et al. 2009](#)), LEDA ([Greenhill & Bernardi 2012](#)), DARE ([Burns et al. 2012](#)), SciHi ([Voytek et al. 2014](#)), BIGHORNS ([Sokolowski et al. 2015](#)), and SARAS ([Patra et al. 2015](#)). Radio interferometers which seek to measure statistical power spectra include the GMRT ([Paciga et al. 2013](#)), LOFAR ([van Haarlem et al. 2013](#)), the MWA ([Tingay et al. 2013](#)), the 21CMA ([Peterson 2004](#), [Wu 2009](#)), and PAPER ([Parsons et al. 2010](#)). The Hydrogen Epoch of Reionization Array (HERA), which is currently being built, is a next-generation instrument that aims to combine lessons learned from previous experiments and is forecasted to be able to make a successful 23σ detection with an eventual 350 elements, using current analysis techniques ([DeBoer et al. 2017](#), [Pober et al. 2014](#)).

The major challenge that faces all 21 cm experiments is isolating a small signal that is buried underneath foregrounds and instrumental systematics that are 4–5 orders of magnitude brighter. A clean measurement therefore requires an intimate understanding of the instrument and a rigorous study of data analysis choices. With continual progress being made in the field and HERA on the horizon, it is becoming increasingly important to understand how the methods we choose interact with each other to affect power spectrum results. In this paper, we discuss three themes essential to a 21 cm power spectrum analysis and how data analysis choices affect each. We approach these themes from a broad perspective, and then perform a detailed case study using data from the 64-element configuration of PAPER.

This paper is organized as follows. In section 2 we introduce the three themes of our focus, using a toy model to develop intuition into each one. Section 3 presents an overview of the PAPER-64 array and observations, highlighting key changes from [Ali et al. \(2015\)](#). Sections 4, 5, and 6 detail how the new PAPER-64 analysis quantifies signal loss, estimates error bars, and eliminates bias, respectively. We conclude in Section 7.

2. POWER SPECTRUM THEMES AND TECHNIQUES

A typical dataset for a 21 cm experiment involves many axes. Visibility measurements, the standard data product for radio telescopes, are saved for many baselines and baseline-types. These visibilities are comprised of many integrations and a spectrum of frequency channels. Data collection can span months and years and can involve multiple polarizations. The data itself contains not only an EoR signal, but layers of bright foregrounds, radio frequency interference, instrumental noise, and other systematics.

The job for 21 cm data analysts is to sift through terabytes of data to ultimately make a power spectrum, a statistical result that encodes the variance of a dataset. In other words, a power spectrum measures the strength of the 21 cm signal on various spatial scales of the sky, a powerful measurement that can be used to trace the evolution of neutral hydrogen during the EoR. There are, however, many data analysis choices that affect both the variance of the dataset itself and how it is measured.

Simply stated, we desire to maximize the sensitivity of a dataset as much as possible, while being confident about the result and able to account for irregularities. There are many choices as a data analyst, such as how to optimally combine time-ordered measurements, how to best and most accurately estimate its variance, and how to weight data in a way that suppresses uninteresting modes while not destroying an EoR signal. Common techniques such as averaging data, inverse covariance weighting, bootstrapping, and jack-knife testing each affect data in different ways and reveal different lessons.

There are often tradeoffs between techniques. For example, [\[cite papers such as Josh's\]](#).

In this paper, we focus on four power spectrum techniques and their affect on three umbrella 21 cm power spectrum themes. We will give brief definitions now, and build intuition for each theme in the sections to follow.

Power Spectrum Techniques

- **Fringe-rate filtering:** The concept of a fringe-rate filter is similar to averaging data in time. We explain our filter in more detail in Section 3, but a broad description is that a fringe-rate filter increases the sensitivity of a dataset and reduces the number of independent samples by an amount dependent on the width of the averaging window.
- **Inverse covariance weighting:** Of the same flavor as inverse variance weighting, inverse covari-

ance weighting weights a dataset by minimizing the covariance between frequency channels. This weighting has the effect of down-weighting correlated information and up-weighting noise-like information.

- **Bootstrapping:** This is a useful method for estimating errors of a dataset from itself. By randomly drawing samples of the data, the spread in those numbers gives us our errors.
- **Jack-Knife testing:** A resampling technique useful for estimating bias, jack-knives can be taken along different dimensions of a dataset to cross-validate results.

Power Spectrum Themes

- **Signal Loss:** As explained in the next session, there are analysis techniques that can lead to the loss of an EoR signal. If not corrected for, it could lead to a false non-detection. Computing signal loss has subtle challenges but is a crucial component for confidence in any result.
- **Error Bar Estimation:** Errors on a 21 cm power spectrum result can make the difference between a detection and a noise-like measurement, which have two very different implications. Errors can be estimated in a variety of ways, and we will discuss a few of them.
- **Bias:** There are several possible sources of bias in a visibility measurement that can leak its way into a power spectrum. It is important to identify them in order to interpret results and develop techniques to suppress contamination.

We will now discuss the three themes more in depth and discuss how certain power spectrum techniques affect each.

2.1. Signal Loss

Signal loss refers to the loss of a cosmological signal in a dataset. It can arise in a variety of ways at multiple stages in an analysis pipeline. Here we focus on signal loss originating from empirically estimating covariance matrices, a method that succeeds in down-weighting foregrounds but can carry the risk of large amounts of signal loss. We will develop our intuition and motivate the effect of signal loss using a toy model simulation.

Suppose we have a very simple dataset which contains 2-dimensional data (representing 100 time integrations and 20 frequency channels). The data is comprised of a sine-wave foreground that varies in time, and a complex, random-noise EoR signal (Figure 1, left).

Before we demonstrate how signal loss can arise, we first look at the eigenspectrum of the covariance matrix that describes our data. That is, if \mathbf{x} is our dataset

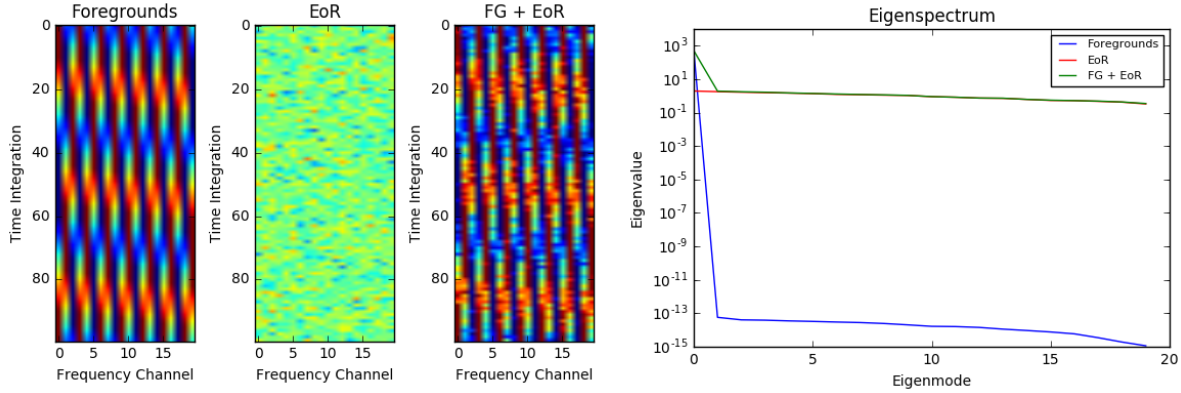


Figure 1. Left: Our toy model dataset contains a sine-wave foreground that varies in time and random noise as an EoR signal. Real parts are shown here. Right: Eigenspectrum of foregrounds only (blue), EoR only (red), and both (green)

which contains both the foreground and EoR, its covariance matrix is empirically defined as $\mathbf{C} \equiv \mathbf{x}\mathbf{x}^\dagger$. The eigenspectrum, which encodes useful information about the strengths of different frequency modes, is shown in the right plot of Figure 1. It is obvious that there is only 1 eigenmode in the foreground-only dataset (since we used one sine-wave), and therefore most of the information in our combined dataset is contained in the first mode.

We would like to use inverse covariance weighting to down-weight the foregrounds in our dataset. To do so, we compute \mathbf{C}^{-1} and use optimal quadratic estimators (see Section 3.2 for more details) to Fourier-transform our data along the ‘frequency’ axis and form a power spectrum. As an explicit check, we use information from only the first eigenmode, and zero out the others. We do this because we know that the foregrounds can be perfectly described by only the first mode, so it should be all that we need to down-weight them.

Figure 2 shows the unweighted (using the identity matrix \mathbf{I} instead of \mathbf{C}) power spectrum for the foreground-only data in blue, the unweighted power spectrum for the EoR-only data in red, and the weighted power spectrum for the combined dataset in green. There is one peak in blue from our one foreground mode.

From the left plot, we see that by down-weighting the first mode, we can perfectly recover EoR. This is in principle the reason why inverse covariance weighting is so attractive for 21 cm data. If we could perfectly model our foregrounds, we could down-weight them without any signal loss. However, this is not the case in reality, since we can’t distinguish between foreground and EoR modes.

If we did not know that our foreground information is contained in only one mode, a naive approach would be to use full inverse covariance weighting (using information from all eigenmodes). Examining this case, our full inverse covariance weighted result (Figure 2, right) almost recovers the EoR signal. It exhibits the correct shape, but the amplitude level is slightly low. This is actually evidence of a small amount of signal loss. In this toy model, the amount of signal loss is small, but

we can exaggerate the effect and investigate its cause by ‘fringe-rate filtering’ our toy model dataset.

Since fringe-rate filtering is similar in practice to averaging in time, we average every 4 time integrations together, yielding 25 independent samples in time (Figure 3, left). We choose these numbers so that the total number of independent samples is similar to the number of frequency channels (our matrices will be full rank). The resulting eigenspectra (Figure 3, right), as compared to those in Figure 1, begin to fall for the last few eigenmodes. Although a subtle feature, it has large consequences on the resulting power spectra.

Applying full inverse covariance weighting to this dataset results in the power spectra shown in Figure 4. It is clear that there is a much larger amount of signal loss for this time-averaged dataset. The subtle drop-off in the eigenspectrum shape suggests that when the spectrum is inverted, a few modes are up-weighted more strongly than the rest. This means that most of our power spectrum information is coming from only the last few modes, and as a result, is a noisier estimate. This is evident by noticing that the green curve in Figure 4 not only exhibits signal loss, but also fails to trace the shape of the unweighted EoR power spectrum.

Using our toy model, we have shown that signal loss can arise from inverse covariance weighting due to unintentionally up-weighting eigenmodes with very small eigenvalues (overfitting the noise). We have also shown that this effect is made larger by reducing the total number of independent samples in a dataset. In reality, 21 cm data from PAPER-64 exhibits ~ 3 orders of magnitude of signal loss when combining the use of an optimal fringe-rate filter and full inverse covariance weighting.

Going back to our time-averaged simulation data, we will now describe several ways to alter the covariance matrix \mathbf{C} in order to avoid signal loss. Recall that \mathbf{C} is computed from the dataset itself, leading to the up-weighting of very noisy, non-existent modes. In practice we compute \mathbf{C} this way because we do not know how to accurately model the matrix. But for our toy model, we know that our simulated, perfectly-noisy EoR should have a covariance matrix that mimics the identity ma-

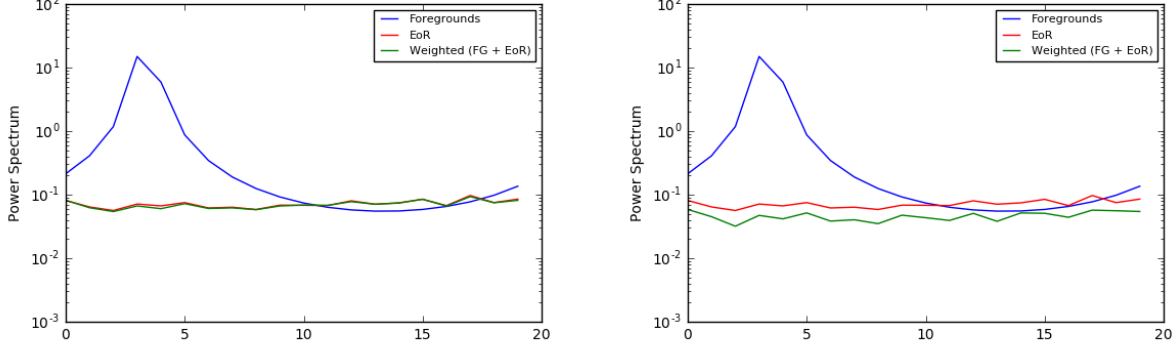


Figure 2. Power spectrum of foregrounds only (blue), EoR only (red), and the combined dataset (green). Contrasted are the effect of using information from the first eigenmode only (left), and full inverse covariance weighting (right).

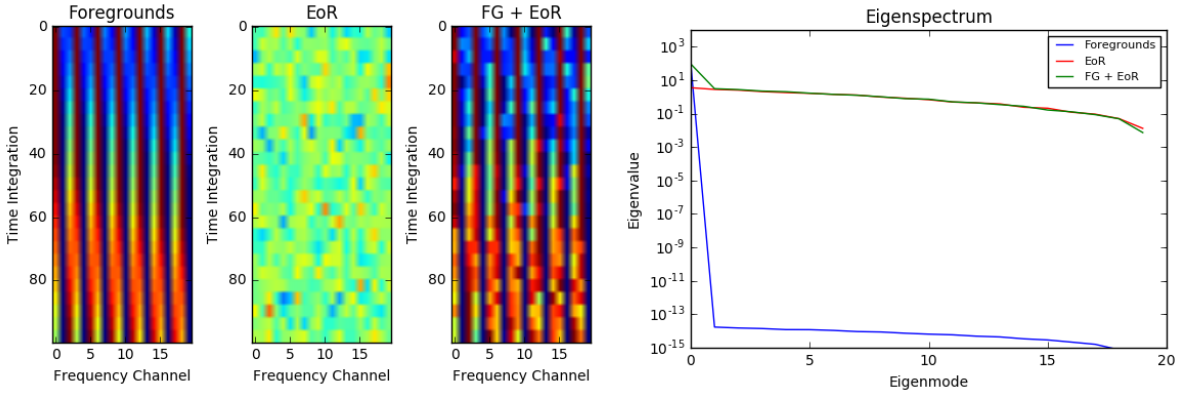


Figure 3. Left: Our ‘fringe-rate filtered’ toy model dataset. It contains 25 independent samples in time. Real parts are shown here. Right: Eigenspectrum of foregrounds only (blue), EoR only (red), and both (green).

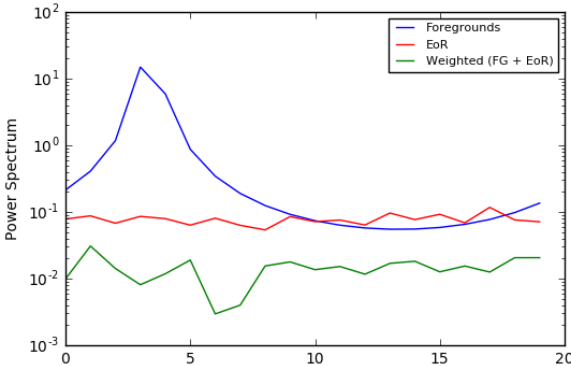


Figure 4. Power spectrum of foregrounds only (blue), EoR only (red), and the full inverse covariance weighted combined dataset (green) for a time-averaged dataset (fewer independent modes).

trix, with its variance encoded along the diagonal. If we model \mathbf{C}_{EoR} as such and add it to $\mathbf{C}_{FG} = \mathbf{x}_{FG}\mathbf{x}_{FG}^\dagger$ to obtain a final \mathbf{C} to use in weighting (instead of computing it based on $(\mathbf{x}_{FG} + \mathbf{x}_{EoR})$), we see that there is no signal loss (Figure 5, upper left).

The next three panels of Figure 5 each involve methods that regularize the matrix \mathbf{C} after it is computed from the foreground + EoR dataset. By regularizing \mathbf{C} , we are flattening out its eigenspectrum. Therefore, some modes will be down-weighted, but the rest will be treated with similar weights. In other words, we won’t be up-weighting the last few noisy modes.

Regularization schemes that we are highlighting here are adding an identity matrix to \mathbf{C} (Figure 5, upper right), killing all but the first three eigenmodes of \mathbf{C} (lower left), and multiplying an identity matrix to \mathbf{C} (lower right). Each avoids signal loss, but it is clear that two of the methods down-weight foregrounds much better than the third. For this toy model, our foregrounds are spread out in frequency and therefore have non-negligible frequency-frequency correlations. Therefore, when multiplying \mathbf{C} by an identity matrix, we are only preserving correlations between the same frequencies. Hence, because we killed off information from all other frequency combinations, we do a poor job suppressing the foreground.

Although this method did not successfully recover EoR for this particular simulation, it is important that we show that there are many options for estimating a covariance matrix, and some may work better than oth-

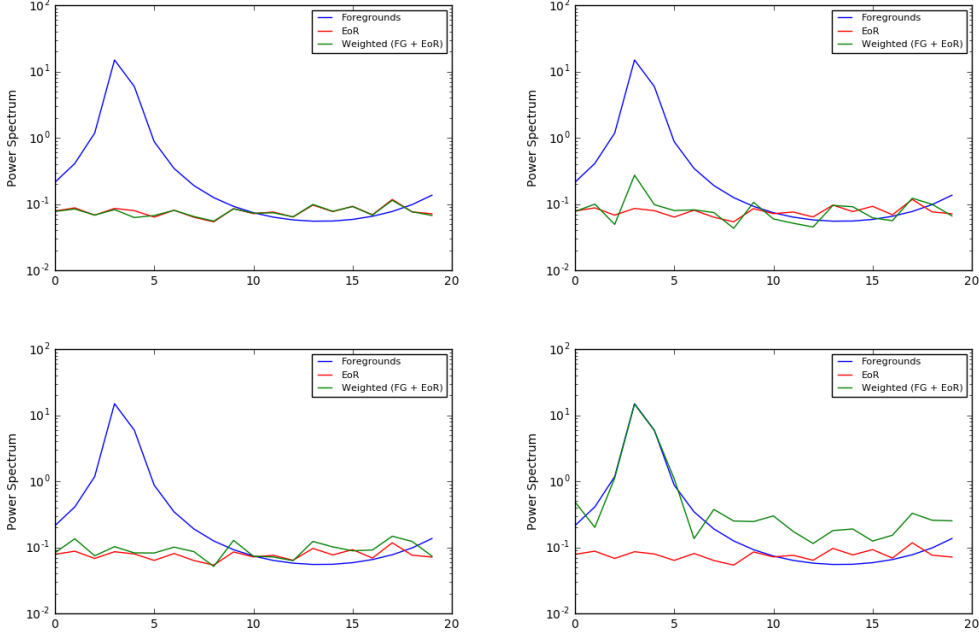


Figure 5. Power spectra of foregrounds only (blue), EoR only (red), and the weighted combined dataset (green). We show four alternate weighting options that each avoid signal loss, including modeling the covariance matrix of EoR (upper left), regularizing \mathbf{C} by adding an identity matrix to it (upper right), using only the first few eigenmodes of \mathbf{C} (lower left), and multiplying an identity matrix to \mathbf{C} (lower right).

ers based on the dataset. One may imagine a situation where a particular systematic is contained to an isolated frequency. In such a case, preserving only the diagonal elements of \mathbf{C} would be an effective way of removing this contamination. In Section 4, we apply the lessons we've learned about signal loss and its interaction with fringe-rate filtering and inverse covariance weighting to PAPER-64 data.

2.2. Error Estimation

2.3. Bias

3. CASE STUDY: PAPER-64

Now that we have developed our intuition regarding signal loss, error estimation, and bias, we will look at each in more detail as applied to data taken by PAPER. We begin with an overview of the telescope array, its observations, and analysis pipeline.

3.1. Observations

The Donald C. Backer Precision Array for Probing the Epoch of Reionization (PAPER) is a dedicated 21 cm experiment located in the Karoo Desert in South Africa. The PAPER-64 configuration consists of 64 dual-polarization drift-scan elements, each 2 m on a side. The antenna layout is formatted in a grid layout (Figure 6), with 8 antennas on a side, 30 m spacing between antennas along the East/West direction, and 4 m spacing between antennas along the North/South direction. For the rest of this paper, we focus on data from only the 30 m pure East/West baselines.

PAPER-64 observed for a total of 135 nights between 2012-2013. The correlator processes a bandwidth of 100-200 MHz, corresponding to a redshift range of 6-12. For more information about the backend system of PAPER-64 and its observations, we refer the reader to [??] and Ali et al. (2015).

Because there is a detailed discussion of the PAPER-64 data reduction pipeline in Ali et al. (2015), here we will only briefly summarize the data processing steps prior to the power spectrum analysis.

Beginning with compressed data products which have been cleaned of radio frequency interference (RFI) at the 6σ level and then down-sampled (to 42.9 s integrations, 203 frequency channels), we then employ the technique of redundant calibration as a means of calibrating for individual antenna gains without needing to use information about the sky. Because PAPER is laid out on a grid, antenna calibration parameters can be found through the use redundancy. Namely, baselines of the same length and orientation should measure the same sky signal, but in practice there are differences due to instrumental effects caused by antennas, cables, and receivers. Using the basis of redundancy, however, allows us to set up a system of equations to solve for a complex gain per antenna that brings all baseline of a particular type into alignment. We do this using the package OMNICAL.

We next solve for the array's overall phase and gain calibration parameters using a standard self calibration method. We used radio sources Pictor A, Fornax A, and the Crab Nebula to fit for an overall phase solution, and

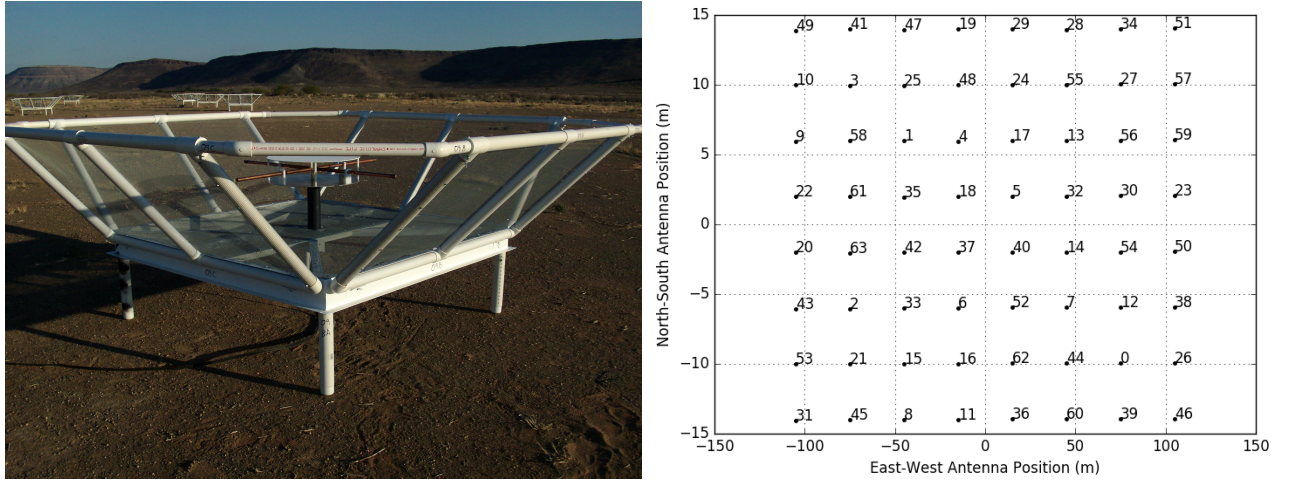


Figure 6. PAPER dipole in South Africa (left) and PAPER-64 antenna layout (right).

set our overall flux scale using Pictor A as a calibrator source. Although PAPER-64 data exists for all 4 polarizations, we only use the xx and yy polarization data to form Stokes I as $V_I = \frac{1}{2}(V_{XX} + V_{YY})$.

Eliminating bright foregrounds remains a challenging yet crucial component of any 21 cm data analysis. There are many techniques to go about foreground removal, including spectral polynomial fitting, principle component analysis, Fourier-mode filtering, non-parametric subtractions, and inverse covariance weighting. PAPER uses a delay-spectrum filtering method which was first explained and applied in Parsons et al. (2014). In short, the delay-filtering technique employs the spectrally smooth nature of foregrounds, which are consequently localized in delay-space, the Fourier dual to frequency. We subtract all components that fall within the horizon limit for a specific baseline type in delay-space, plus a 15 ns buffer, thus gaining about ~ 4 orders of magnitude in sensitivity.

After removing an additional layer of RFI (values 3σ above the median), we average together all our data into two datasets: even julian dates and odd julian dates. A total of 124 nights of data comprises this average.

Finally, our last analysis step before power spectrum estimation is the use of a fringe-rate filter. As shown in Parsons et al. (2016), a fringe-rate filter allows us to maximize our sensitivity even further by averaging visibilities in time. We apply this filter in the fringe-rate domain, the Fourier-dual to time, and it effectively amounts to increasing our data's integration time. Another way to describe the filter is that it weights different parts of the sky (which rotate at different "fringe-rates") by the antenna beam. This allows us to up-weight parts of the sky high in the primary beam, and down-weight those that are less sensitive. In practice, the optimal fringe-rate profile is computed for a fiducial 30 m baseline at 150 MHz, the center frequency in our band. The filter is implemented on a per baseline basis by convolving the time-domain visibilities with the Fourier transform of the fringe-rate filter, resulting in averaged visi-

bilities yielding ~ 2 orders of magnitude in sensitivity.

3.2. Power Spectrum Estimation

To form power spectrum quantities using our two fringe-rate filtered, LST-binned datasets, we use OQE methods as described by [??]. A summary of the method is as follows.

We begin with our data vector \mathbf{x} , which contains our visibilities that have the shape (*times, frequencies*) for each baseline and data group ('even' or 'odd'). As part of our bootstrapping routine (and to speed things up), we divide up our total number of baselines into 5 random, equal-sized groups. Taking \mathbf{x} to be averaged data from all baselines within a group, we now have 10 possible data vectors (for 5 groups and 2 datasets). We next form the quantity \hat{q}_α :

$$\hat{q}_\alpha = \frac{1}{2} \mathbf{x}^\dagger \mathbf{C}^{-1} \mathbf{Q}_\alpha \mathbf{C}^{-1} \mathbf{x} - b_\alpha \quad (1)$$

where \mathbf{C} is the covariance matrix defined to be $\mathbf{C} \equiv \langle \mathbf{x} \mathbf{x}^\dagger \rangle$. The matrix \mathbf{Q} is an operator that takes our frequency-domain visibilities and Fourier-transforms them into power spectrum space. A noise bias b_α is subtracted off. The index α represents each k_{\parallel} bin, where k_{\parallel} is the Fourier-dual to frequency.

Notice that there are two quantities of $\mathbf{C}^{-1} \mathbf{x}$ in the expression for \hat{q} , representing two copies of inverse covariance weighted data. We perform all possible cross-multiplications of this quantity, except between the same datasets ('even' with 'even', for example) and same groups ('baseline group 1' with 'baseline group 1', for example). We avoid these computations to prevent the introduction of biases from shared auto power.

Finally, we normalize our power spectrum estimates using the matrix \mathbf{M} :

$$\hat{\mathbf{p}} = \mathbf{M} \hat{\mathbf{q}} \quad (2)$$

where $\hat{\mathbf{p}}$ is the normalized estimate of the true power spectrum \mathbf{p} . We compute \mathbf{M} using the Fisher matrix \mathbf{F} , defined as:

$$\mathbf{F}_{\alpha\beta} = \frac{1}{2} \text{tr}(\mathbf{C}^{-1} \mathbf{Q}_\alpha \mathbf{C}^{-1} \mathbf{Q}_\beta). \quad (3)$$

$$(4)$$

We have a choice for \mathbf{M} , and we choose to compute it by taking the Cholesky decomposition of \mathbf{F} . Namely, we decompose the Fisher matrix such that $\mathbf{F} = \mathbf{LL}^\dagger$, where \mathbf{L} is a lower triangular matrix. Next, we construct $\mathbf{M} = \mathbf{DL}^{-1}$, where \mathbf{D} is a diagonal matrix. Hence, our window function $\mathbf{W} = \mathbf{MF}$ becomes $\mathbf{W} = \mathbf{DL}^\dagger$ and is an upper triangular matrix. This window function was constructed in a way to prevent the leakage of foreground power from low k to high k modes. Specifically, we order the elements in \mathbf{F} in such a way so that power can leak from high k modes to low k modes, but not vice versa. Since most foreground power shows up at low k 's, this method ensures a window function that retains clean, noise-dominated measurements.

Finally, our final power spectrum is:

$$\hat{\mathbf{p}} = \mathbf{W}\mathbf{p} \quad (5)$$

In practice, we end up with a 2-dimensional power spectrum quantity, which is a function of both time and k . We compute 20 bootstraps of these quantities, where each bootstrap creates baseline groups randomly. We form both the quantity $\mathbf{P}(\mathbf{k})$ and the folded version $\Delta^2(\mathbf{k})$, defined as:

$$\Delta^2(\mathbf{k}) = \frac{k^3}{2\pi^2} \hat{\mathbf{p}}(\mathbf{k}) \quad (6)$$

4. APPLICATION: SIGNAL LOSS

4.1. Noise and EoR

One critical new component of our power spectrum pipeline is that we have many different power spectrum channels that simultaneously get processed at the same time and are especially useful for signal loss (Section 4) and sensitivity (Section ??) verification. Two important channels, in addition to our PAPER-64 data, are a noise dataset and an EoR dataset (in addition to these, we do different combinations of all three). We will briefly describe each.

We create random noise with a scale determined by the sensitivity of our instrument and parameters of our dataset. We calculate our system temperature for our frequencies of interest as:

$$T_{sys} = 180 \left(\frac{\nu}{0.18} \right)^{-2.55} + T_{rcvr} \quad (7)$$

where ν are frequencies in GHz. We use a receiver temperature of 200 K, yielding $T_{sys} = 487$ at 150 MHz. This is lower than in [Ali et al. \(2015\)](#) because [why?]. We convert this temperature into a variance statistic using:

$$T_{rms} = \frac{T_{sys}}{\sqrt{\Delta\nu \Delta t N_{days} N_{pol}}} \quad (8)$$

where $\Delta\nu$ is channel spacing, Δt is integration time, N_{days} is the number of data samples for a particular time and frequency that went into our LST binned set, and N_{pol} is the number of polarizations (2 for Stokes I). Our simulated noise has the same shape as our data, and we fringe-rate filter it in the same way to best mimic the real noise floor of our data.

A second additional important channel in our pipeline is a simulated EoR signal. We again simulate random noise (with a default scale of 1) with the same shape as our data, and we fringe-rate filter this signal twice. The first filter transforms the unattached noise into a signal that's attached to the sky (what our instrument observes). The second filter represents the fringe-rate filtering step in our data analysis pipeline. As described in Section 4, we create an EoR signal at various amplitude levels.

Our multi-channel power spectrum pipeline has been essential in helping us understand the nuances in our pipeline. Because there are many different components and countless subtle effects affecting our final limits, it has been imperative to carry all our channels through the analysis to validate each step.

4.2. Signal Loss Methodology

Based on our analysis pipeline, potential signal loss is a real and significant issue. More specifically, when applying inverse covariance weighting, \mathbf{C}^{-1} is empirically estimated from the data itself, which has the consequence of over-fitting the noise in the data, producing power spectra values well below the thermal noise limit that is predicted based on observation parameters. This is especially prevalent when weighting fringe-rate-filtered data, which has so few independent time modes to begin with, leading to a noisier dataset. Being able to accurately quantify this loss is crucial in interpreting and providing credibility to any power spectrum limits.

New to the PAPER-64 analysis is a robust method to estimate signal loss associated with inverse covariance weighting. This method, explained below, is now a standard analysis step for all PAPER analyses and one that will be used for HERA moving forward.

As discussed previously, our power spectrum pipeline runs on a standardized set of channels (pure data, pure noise, pure EoR, and combinations of the three). As part of our signal loss routine, we also compute power spectra with various levels of the created EoR signal, dialing its amplitude from well-below the data level, to well-above. Suppose that \mathbf{e} is the injected EoR (at some amplitude level), and \mathbf{x} is our data vector. We define \mathbf{r} to be:

$$\mathbf{r} = \mathbf{x} + \mathbf{e} \quad (9)$$

Using our OQE formalism, we are interested in the following two quantities: P_{in} and P_{out} . The input power spectrum, P_{in} represents the unweighted power spectrum of only \mathbf{e} , our simulated EoR signal. The output power spectrum, P_{out} , is the weighted power spectrum

of \mathbf{e} that would result from our pipeline if the signal was mixed with our data. Comparing the two quantities yields insight into how much of \mathbf{e} is lost due to our choice of weighting. Ignoring normalization, factors:

$$P_{in} \propto \mathbf{e}^\dagger \mathbf{I}^{-1} \mathbf{Q} \mathbf{I}^{-1} \mathbf{e} \quad (10)$$

$$\begin{aligned} P_{out} &\equiv \mathbf{P}_e = \mathbf{P}_r - \mathbf{P}_x \\ &\propto \mathbf{r}^\dagger \mathbf{C}_r^{-1} \mathbf{Q} \mathbf{C}_r^{-1} \mathbf{r} - \mathbf{x}^\dagger \mathbf{C}_x^{-1} \mathbf{Q} \mathbf{C}_x^{-1} \mathbf{x} \end{aligned} \quad (11)$$

It is noted that the output power spectrum is comprised of two terms: the covariance treated power spectrum associated with \mathbf{r} , and that of data \mathbf{x} alone.

One may wonder why P_{out} cannot be computed simply as the weighted power spectrum of \mathbf{e} alone, namely $P_{out} \propto \mathbf{e}^\dagger \mathbf{C}_e^{-1} \mathbf{Q} \mathbf{C}_e^{-1} \mathbf{e}$. Expanding Equation 11:

$$\begin{aligned} P_{out} &\propto (\mathbf{x} + \mathbf{e})^\dagger \mathbf{C}_r^{-1} \mathbf{Q} \mathbf{C}_r^{-1} (\mathbf{x} + \mathbf{e}) - \mathbf{x}^\dagger \mathbf{C}_x^{-1} \mathbf{Q} \mathbf{C}_x^{-1} \mathbf{x} \\ &\propto \mathbf{x}^\dagger \mathbf{C}_r^{-1} \mathbf{Q} \mathbf{C}_r^{-1} \mathbf{x} + \mathbf{e}^\dagger \mathbf{C}_r^{-1} \mathbf{Q} \mathbf{C}_r^{-1} \mathbf{e} + \mathbf{x}^\dagger \mathbf{C}_r^{-1} \mathbf{Q} \mathbf{C}_r^{-1} \mathbf{e} \\ &\quad + \mathbf{e}^\dagger \mathbf{C}_r^{-1} \mathbf{Q} \mathbf{C}_r^{-1} \mathbf{x} - \mathbf{x}^\dagger \mathbf{C}_x^{-1} \mathbf{Q} \mathbf{C}_x^{-1} \mathbf{x} \end{aligned}$$

And taking the case of very large \mathbf{e} , so that $\mathbf{C}_r^{-1} \sim \mathbf{C}_e^{-1}$ and any terms involving only \mathbf{x} are small:

$$\begin{aligned} P_{out, e \gg x} &\propto \mathbf{e}^\dagger \mathbf{C}_e^{-1} \mathbf{Q} \mathbf{C}_e^{-1} \mathbf{e} + \mathbf{x}^\dagger \mathbf{C}_e^{-1} \mathbf{Q} \mathbf{C}_e^{-1} \mathbf{e} \\ &\quad + \mathbf{e}^\dagger \mathbf{C}_e^{-1} \mathbf{Q} \mathbf{C}_e^{-1} \mathbf{x} \end{aligned} \quad (12)$$

We see that our naive expression for P_{out} is the first term, but there also two additional terms. An initial assumption would be that the cross-terms that involve both \mathbf{e} and \mathbf{x} should be zero, since the two quantities are un-correlated. However, [need explanation about power in cross-terms here]. Therefore, in our investigation of signal loss, we use the full quantity for P_{out} as in Equation 11.

For the unweighted case ($\mathbf{C} \equiv \mathbf{I}$), we expect P_{out} and P_{in} to be equal, and hence the ratio of P_{in}/P_{out} to be 1. For the weighted case, this is not true due to signal loss. In order to quantify the loss, we look at the ratio of P_{in} to P_{out} as the amplitude level of the injected signal \mathbf{e} is increased. In the next section, we highlight two methods that yield similar results for the determination of signal loss using P_{in} and P_{out} .

4.3. Signal Loss in Practice

Recall that fringe-rate filtered noise, which mimics the level of noise in our actual PAPER-64 dataset, is a channel in our power spectrum pipeline. We can compute signal loss quantities of interest for the noise \mathbf{n} similar to the expressions we featured previously for data \mathbf{x} .

$$P_{in} \propto \mathbf{e}^\dagger \mathbf{I}^{-1} \mathbf{Q} \mathbf{I}^{-1} \mathbf{e} \quad (13)$$

$$\mathbf{s} = \mathbf{n} + \mathbf{e} \quad (14)$$

$$P_{out} \propto \mathbf{s}^\dagger \mathbf{C}_s^{-1} \mathbf{Q} \mathbf{C}_s^{-1} \mathbf{s} - \mathbf{n}^\dagger \mathbf{C}_n^{-1} \mathbf{Q} \mathbf{C}_n^{-1} \mathbf{n} \quad (15)$$

Using the input and output power spectra for range of EoR amplitudes, we use two methods to determine signal loss associated with the over-fitting of noise during inverse covariance weighting. We first look at signal loss for the pure noise case (no data), to show that we can successfully inject EoR signals, determine signal loss, and then recover the signal.

The first method is very straightforward. Post-bootstrapping, our final power spectra are 1-dimensional and only a function of k . For each k , we simply look at P_{out} as a function of P_{in} , as shown in Figure 7. The shape of this function can be explained as follows. At small injection levels (small \mathbf{e}), P_{out} and P_{in} are equal, and there is no signal loss. As the amplitude of EoR increases, we then move into a regime where the final output power spectrum is lower than the unweighted input one. This is dangerous, because without correcting for this effect one might be led to underestimate the EoR signal. The peculiar tail at very low injection levels (where $P_{out} > P_{in}$) is an unphysical feature, but rather illustrates that there is some non-negligible cross-term power between \mathbf{n} and \mathbf{e} .

For this method, we interpolate the signal loss factor (per k), computed as P_{in}/P_{out} , at a P_{out} value equal to the 2σ power spectrum upper limit of noise alone. In other words, we look at $P_{noise} \propto \mathbf{n}^\dagger \mathbf{C}_n^{-1} \mathbf{Q} \mathbf{C}_n^{-1} \mathbf{n}$, compute its 2σ upper limit (mean over bootstraps + $2\times$ standard deviation over bootstraps), and interpolate the value of P_{in}/P_{out} at this value. We therefore end up with one signal loss correction factor per k .

Figure 8 shows the power spectrum of our noise simulation, using full inverse covariance weighting, both before and after signal loss correction. Prior to signal loss correction, it is obvious that the power spectrum is unfeasible because it is well below the theoretical noise level prediction. Post-correction, the power spectrum values blow up much higher than both the theory and unweighted power spectrum. This is an effect caused by the steep nature of the eigenspectrum of \mathbf{C} , and is explained more in Section 4.4.

[Need a plot that shows our signal loss factors are CORRECT. How to do that??]

Our second method for estimating signal loss is similar to the first, but more comprehensive in a statistical sense. Instead of looking at input and output power spectra after bootstrapping, we now look at their values for every bootstrap in order to get a sense of their distributions. Figure 9 plots P_{in} vs. P_{out} for 20 bootstraps, and as expected, the function now has a spread in the width-direction in comparison to what was plotted in Figure 7, but otherwise shows a familiar trend. Similarly, our weighted noise power spectra also has a defined spread due to bootstrapping.

Using these two distributions (P_{in}/P_{out} and P_{noise}), we can create bins along the P_{noise} axis to yield histograms of signal loss factors for each bin. We similarly sort the values of P_{noise} into the same bins, and multiply the probability of P_{noise} per bin (the number of

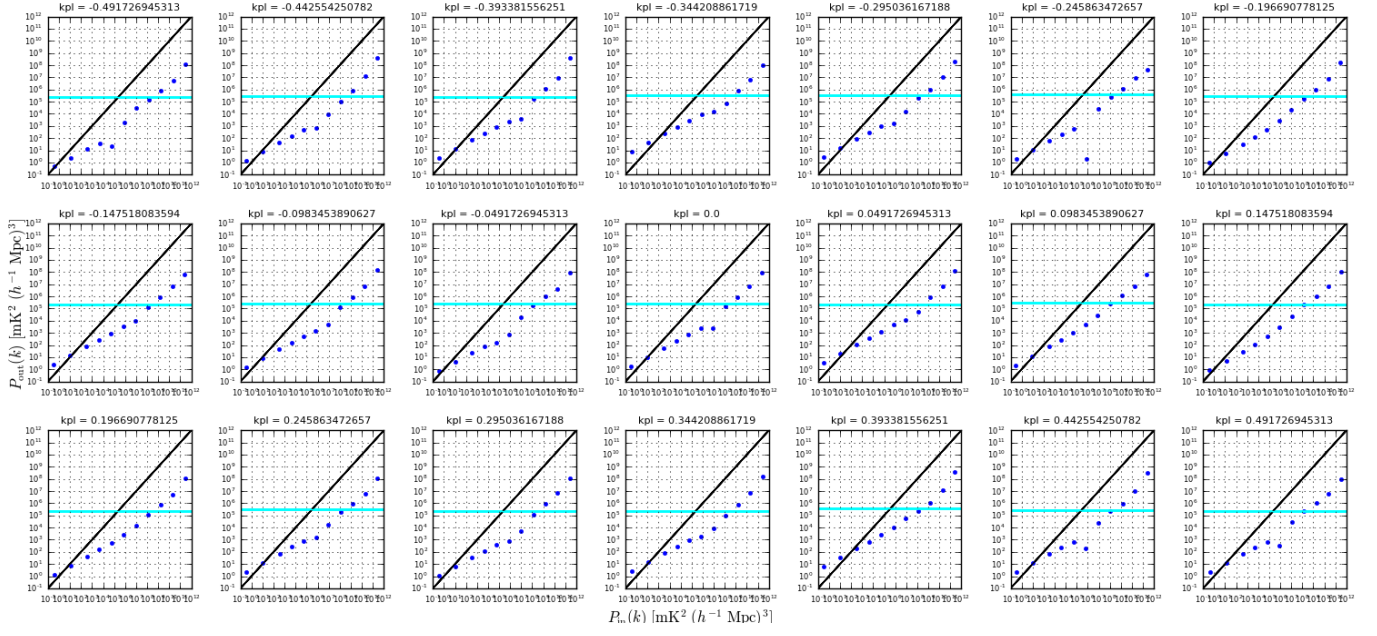


Figure 7. P_{in} vs. P_{out} (blue points) for 15 injection levels and 21 k 's. The solid cyan line is the 2σ upper limit for the weighted power spectrum of noise alone, and it is at this level where the signal loss factor P_{in}/P_{out} is computed by interpolation. [Maybe re-do this plot with closer-together points]

values falling into that bin, divided by the total) with the signal loss factors in that bin, essentially computing a weighted average across all bins to obtain a final signal loss factor per k . As shown in Figure 10, the results are very similar to the previous method. For future power spectrum results, we choose to use the second method because it computes final signal loss values using our full distributions of measurements.

One thing to note is that for both methods, we have been careful to validate that the computations yield no signal loss (signal loss factors of 1) for the unweighted power spectrum case, as is expected. This is important in confirming that signal loss is a direct result of the choice for \mathbf{C} .

4.4. Data Weighting

With our signal loss formalism established, we now have the capability of experimenting with different weighting options for \mathbf{C} . Our goal here is to choose a weighting method that successfully down-weights foregrounds and systematics in our data without generating large amounts of signal loss. We have found that the balance between the two is a delicate one and requires [?? finish sentence...].

We now turn our attention to power spectra using the 30 m East/West baselines of PAPER-64. Our dataset spans 8.5 hours of LST (.1-8.6 hrs), includes a total of 51 baselines, and is fringe-rate filtered using an optimal fringe-rate filter. We have two datasets (even days and odd days), and only cross-multiply data from different days and different baselines. We are interested in 21 frequency channels (channels 95-115), which yields a power spectrum for a redshift of $z = 8.4$.

Using full inverse covariance weighting, our results are not too dissimilar to that of pure noise. Signal loss factors (Figure 11) are of similar order of magnitude, and our power spectrum blows up past the unweighted version after signal loss correction (Figure 12).

Looking into this behavior in more detail, we investigate the shape of the eigenspectrum of \mathbf{C} for a typical baseline used in the analysis. Figure 13 shows this spectrum for baseline (1,4). Most obviously, the spectrum is steep, spanning 4 orders of magnitude. Not as obvious is the effect of this shape on our results. When the matrix \mathbf{C} is inverted to form \mathbf{C}^{-1} , the effect of the steepness of the eigenspectrum is to up-weight very few modes of the sky while the rest are drastically down-weighted. More specifically, our fringe-rate filtered data contains a finite, small number of independent modes, thereby resulting in a covariance matrix that can be described by just a few modes. Beyond the first few modes, the eigenvalues of each additional mode falls off dramatically. When inverting, we end up not only down-weighting those initial modes but severely up-weighting a few insignificant ones. Because of our weighting choice, signal loss blows up as it thinks we only have a couple modes in our data.

Clearly the full inverse covariance treatment of our data is suboptimal to even the unweighted case, but we would like to find a weighting method that does successfully down-weight contaminants in our data and make some improvement over the unweighted power spectrum. There are many choices for determining the covariance matrix \mathbf{C} , but here we will illustrate [?] promising ones as applied to PAPER-64.

[TO DO: decide on/explain/show different weightings]

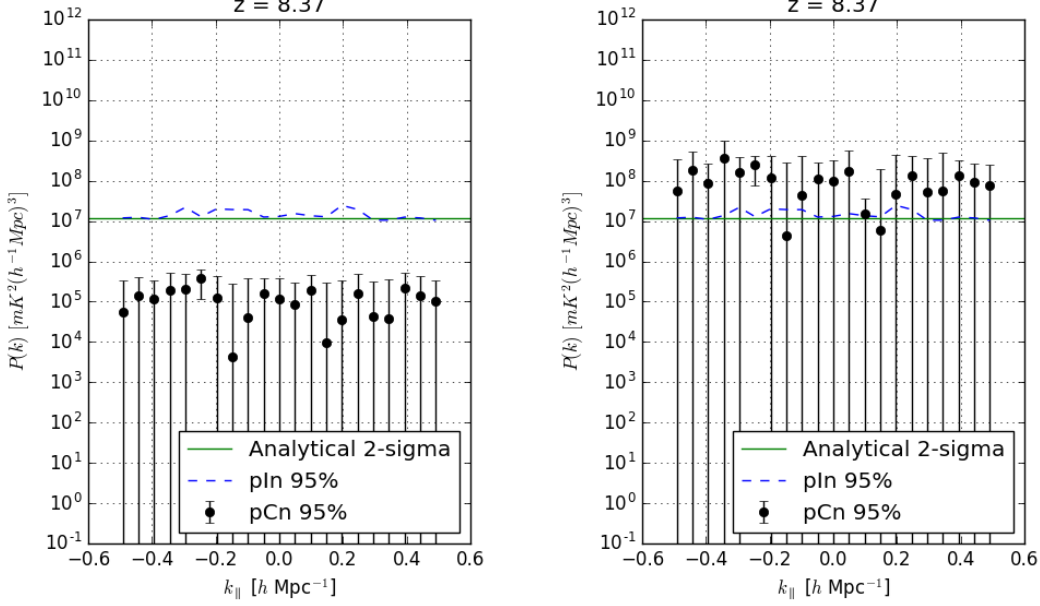


Figure 8. Full inverse covariance weighted power spectrum of pure noise (black points, with 2σ error bars) before signal loss correction (left) and after (right). The dashed blue line is the unweighted power spectrum (2σ upper limit). The solid green line is the theoretical noise level prediction based on observational parameters. [Color negative points grey]

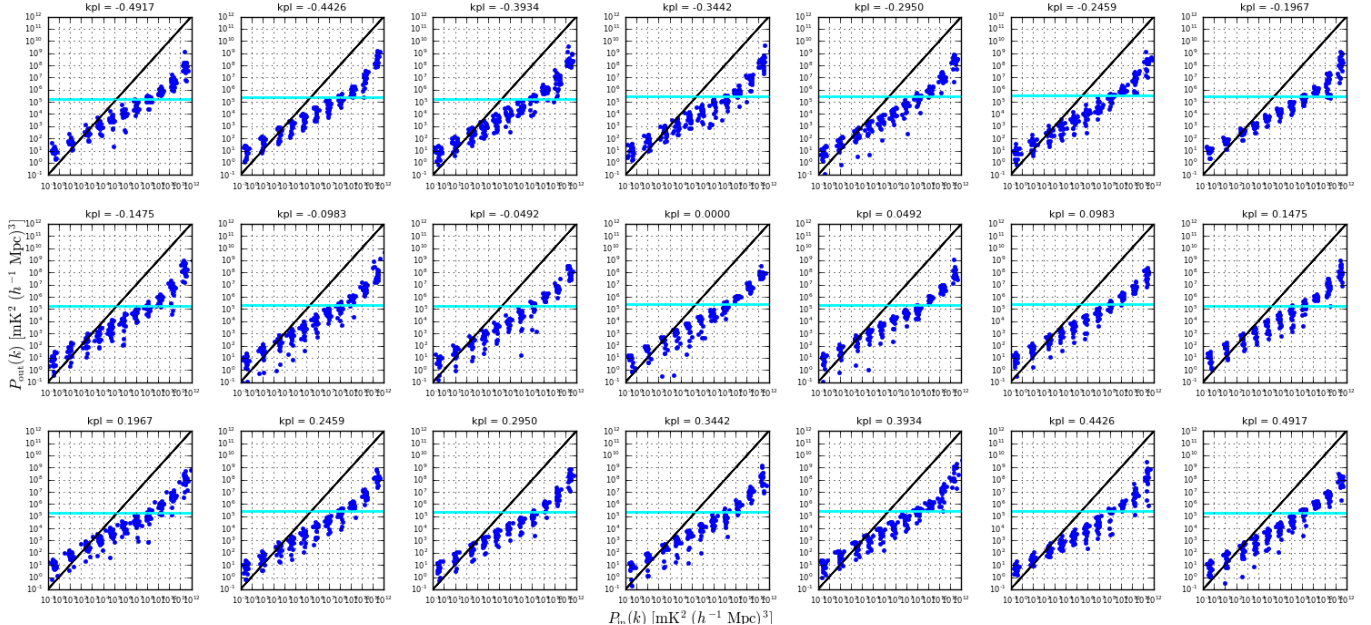


Figure 9. P_{in} vs. P_{out} (blue) for 15 injection levels, 20 bootstraps, and 21 k 's. [Plot a semi-transparent cyan range of pCn values instead of just the max]

5. APPLICATION: ERROR ESTIMATION

5.1. Thermal Noise

[Add info on sensitivity equation, how we calculate effective intime and adjust beam factor because of FRF, etc.]

5.2. Bootstrapping

[Include info about baseline bootstrapping:]

For the Ali et al. (2015) method, each group is then sampled with replacement to create a new group, of the same size, that can have repeated baselines inside it. We discover that in doing so, we are sacrificing some of our sensitivity since this results in there being 3-4 repeated baselines per group. In order to maximize our sensitivity but still apply random sampling for use in error estimation, we instead form new groups using all independent

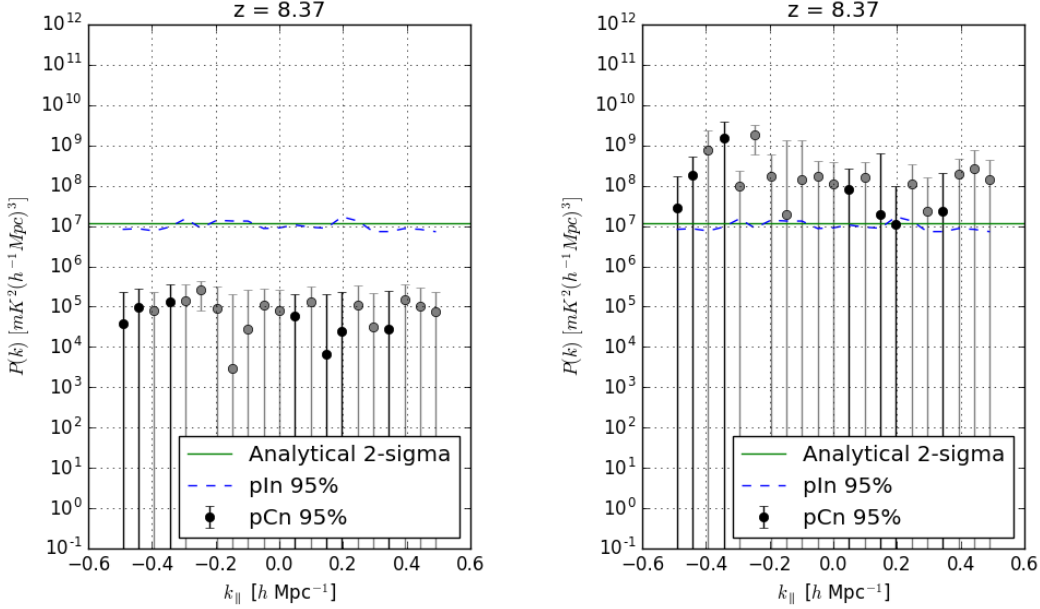


Figure 10. Full inverse covariance weighted power spectrum of pure noise (black and grey points, with 2σ error bars) before signal loss correction (left) and after (right). Black points correspond to positive values, while grey points correspond to originally negative values that have been made positive for plotting. The dashed blue line is the unweighted power spectrum (2σ upper limit). The solid green line is the theoretical noise level prediction based on observational parameters.

baselines except the very last one. For example, if we have 10 baselines in a group, we use the first 9 to guarantee at least 9 independent measurements, and then fill the last slot randomly out of the 10. We do this for all 5 groups. This is still a valid means of bootstrapping because there are many more possibilities of baseline groupings than the number of bootstraps we run for this analysis ($nboots = 20$).

[Include info about second round of bootstrapping:] In Ali et al. (2015), a second round of bootstrapping occurs over the bootstrap and time axes simultaneously. Random values are sampled with replacement along both axes, drawing as many values as there are number of bootstraps and times. Final power spectrum limits are then computed by taking the mean and standard deviation over this second bootstrap axis.

However, we have found that this method greatly underestimates power spectrum errors, especially for fringe-rate filtered data. This can be explained by the fact that fringe-rate filtered data has a dramatically reduced number of independent modes. Hence, drawing 100 samples out of a length-100 dataset that only has 5 independent modes in it, for example, results in a narrower distribution of values that leads to a false error estimation.

To avoid this issue, we instead take a simple average along the time axis. Our final power spectrum limits are

computed by taking the mean and standard deviation over our single bootstrap axis.

6. APPLICATION: BIAS

[Include info about optimal FRF:] In Ali et al. (2015), the filter applied was degraded (widened in fringe-rate space) from an optimal one that can be constructed based on the integration time of the data. This was chosen to decrease the resulting integration time, therefore increasing the number of independent modes and reducing signal loss associated with applying optimal quadratic estimators (OQE) on data with too few modes.

New to our updated PAPER-64 analysis is the use of the optimal fringe-rate filter, which maximizes our sensitivity. With the development of a robust method for assessing signal loss (see Section 4), we feel comfortable using a narrow filter (Figure 14), resulting in an effective integration time of 3857 s (see Section ?? for calculation) and 8 total independent modes for our 8.5 hours of LST.

7. CONCLUSION

8. ACKNOWLEDGEMENTS

[NSF Graduate Research Fellowship Program (GRFP) Fellowship] [UC Berkeley Chancellor's Fellowship]

REFERENCES

Ali, Z. S., et al. 2015, ApJ, 809, 61

Bowman, J. D., & Rogers, A. E. E. 2010, Nature, 468, 796

Burns, J. O., et al. 2012, Advances in Space Research, 49, 433

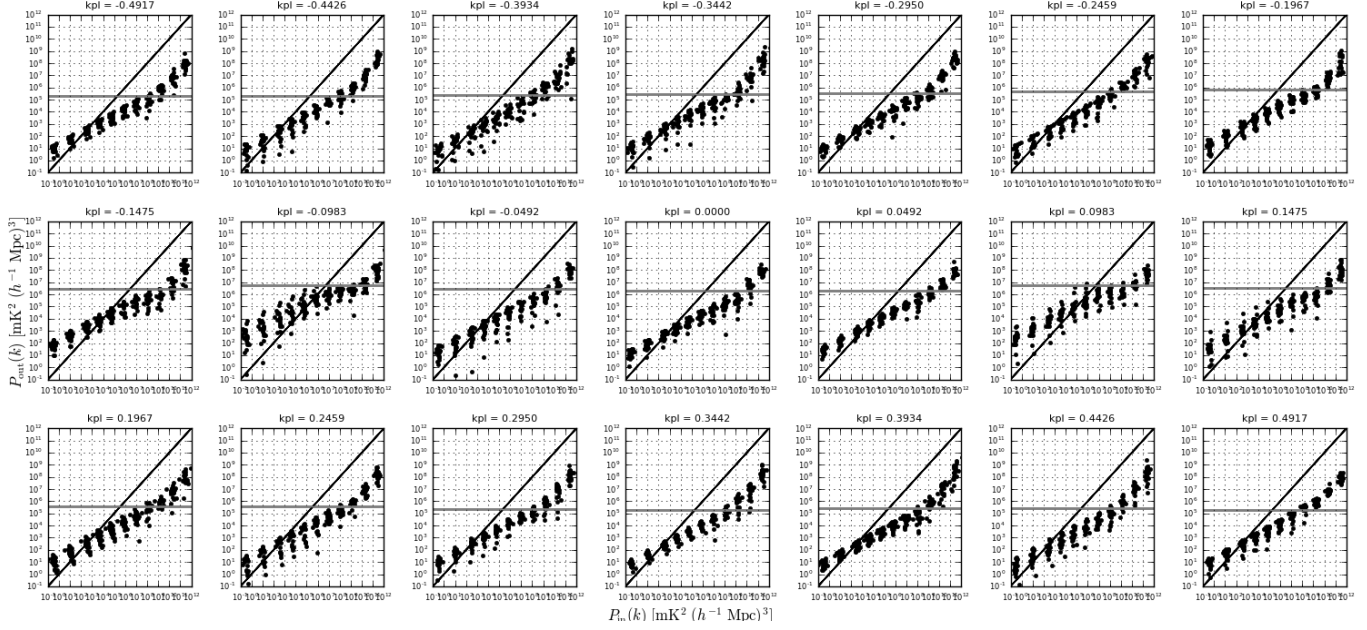


Figure 11. P_{in} vs. P_{out} (black) for 15 injection levels, 20 bootstraps, and 21 k 's. [Plot a semi-transparent grey range of pCv values instead of just the max]

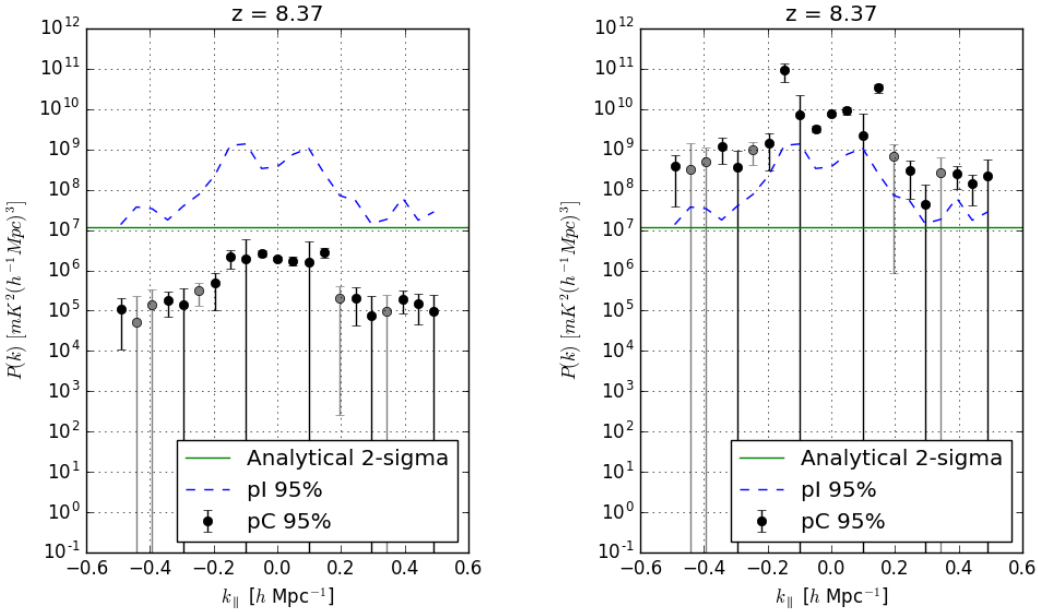


Figure 12. Full inverse covariance weighted power spectrum of PAPER-64 data (black and grey points, with 2σ error bars) before signal loss correction (left) and after (right). Black points correspond to positive values, while grey points correspond to originally negative values that have been made positive for plotting. The dashed blue line is the unweighted power spectrum (2σ upper limit). The solid green line is the theoretical noise level prediction based on observational parameters.

- DeBoer, D. R., et al. 2017, Publications of the Astronomical Society of the Pacific, 129, 045001
 Ellingson, S. W., Clarke, T. E., Cohen, A., Craig, J., Kassim, N. E., Pihlstrom, Y., Rickard, L. J., & Taylor, G. B. 2009, IEEE Proceedings, 97, 1421
 Greenhill, L. J., & Bernardi, G. 2012, ArXiv e-prints
 Paciga, G., et al. 2013, MNRAS
 Parsons, A. R., Liu, A., Ali, Z. S., & Cheng, C. 2016, ApJ, 820, 51

- Parsons, A. R., et al. 2010, AJ, 139, 1468
 —. 2014, ApJ, 788, 106
 Patra, N., Subrahmanyam, R., Sethi, S., Udaya Shankar, N., & Raghunathan, A. 2015, ApJ, 801, 138
 Peterson, U.-L. P. X.-P. W. J. 2004, ArXiv Astrophysics e-prints
 Pober, J. C., et al. 2014, ApJ, 782, 66
 Sokolowski, M., et al. 2015, PASA, 32, e004
 Tingay, S. J., et al. 2013, PASA, 30, 7
 van Haarlem, M. P., et al. 2013, A&A, 556, A2

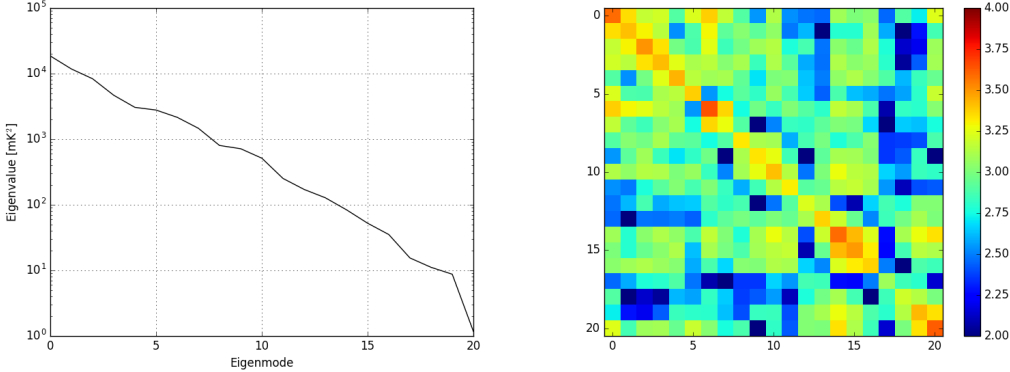


Figure 13. Eigenspectrum for \mathbf{C} for baseline (1,4) for the 21 channels of interest (left) and covariance matrix \mathbf{C} for the same baseline (right).

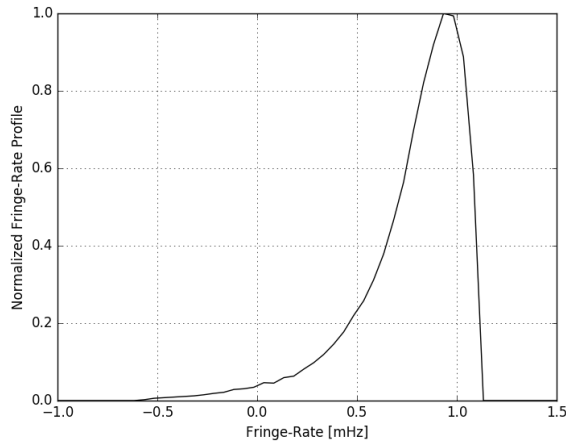


Figure 14. The optimal fringe-rate filter used in the analysis, normalized to 1.

Voytek, T. C., Natarajan, A., Jáuregui García, J. M., Peterson, J. B., & López-Cruz, O. 2014, ApJL, 782, L9
 Wu, X. 2009, in Bulletin of the American Astronomical Society, Vol. 41, American Astronomical Society Meeting Abstracts #213, 474